Optimizing eddy kinetic energy in Veros

The impact of tuning the parametrisation of turbulent mesoscale eddies using Bayesian Optimization in the ocean model Veros

Bachelor thesis

Written by *Asger Thormann*

January 12, 2025

Supervised by
Markus Jochum and Marta Mrozowska

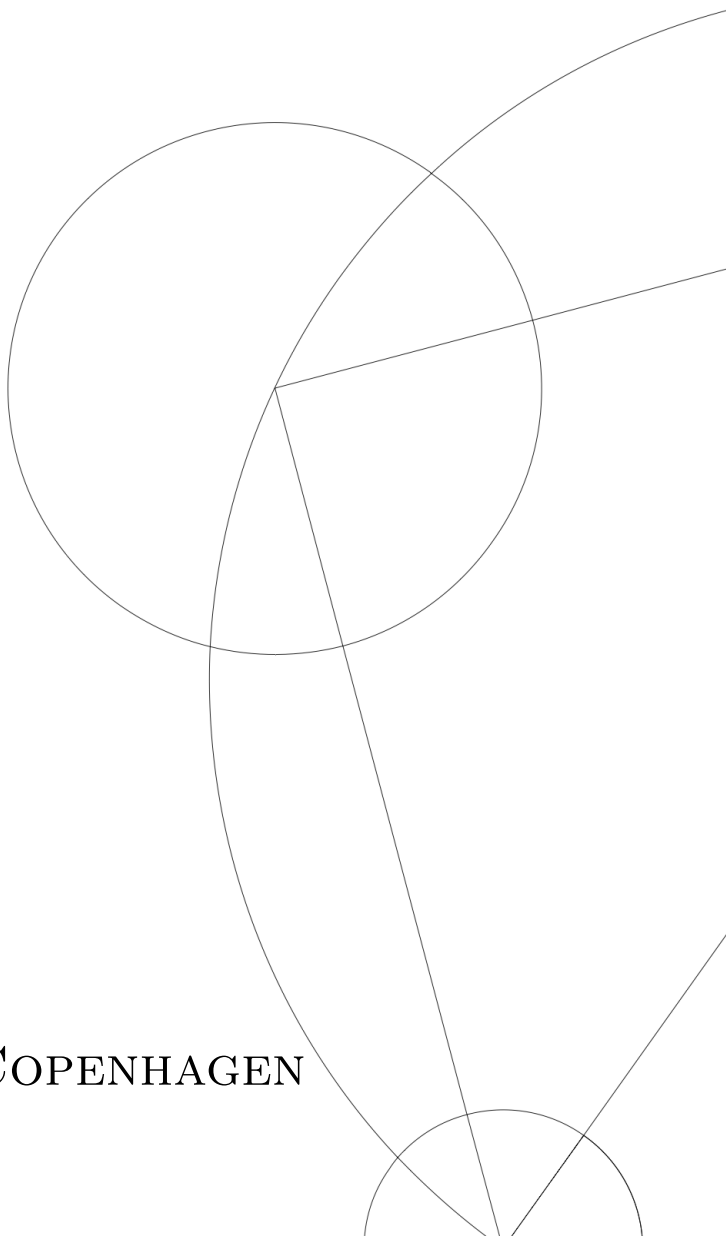

University of Copenhagen

UNIVERSITY OF COPENHAGEN

Name of Institute:	Niels Bohr Institute
Name of Department:	PICE
Author(s):	Asger Thormann
Email:	kfw373@alumni.ku.dk
Title and subtitle:	Optimizing eddy kinetic energy in Veros - The impact of tuning the parametrisation of turbulent mesoscale eddies using Bayesian Optimization in the ocean model Veros
Supervisor(s):	Markus Jochum and Marta Mrozowska
Handed in:	13.01.2025
Defended:	23.01.2025

Name _____ Name _____

Signature _____ Signature _____

Date _____ Date _____

Abstract

This study aims to optimize the parameter set (c_k and c_ϵ) controlling the sources and sinks of the Gent-McWilliams parametrisation of eddy kinetic energy (EKE) minimizing Mixed Layer Depth (MLD) bias in the southern ocean, while maintaining the strength of the Antarctic Circumpolar Current (ACC).

By applying the optimization tool Veropt, which uses a Bayesian optimization method, to the ocean model Veros and using MLD and the strength of the ACC (137 Sv) as targets, parameters are found resulting in a combined error of 0.44 and 0.36 dependent on the chosen MLD target. The study finds that the optimization result is highly dependent on the chosen target as optimal parameters vary by several orders of magnitude. Analysis of EKE and thickness diffusivity (K_{gm}) for the optimized parameters conclude that there is an optimal level of EKE that differs by two orders of magnitude between the experiments, which makes it dependent on the targets used. In conclusion the MLD biases in the southern ocean can be optimized by tuning c_k and c_ϵ but the processes concerning these are not fully captured by the parametrisation scheme and there are most likely unresolved processes affecting these targets.

Contents

1 Introduction

On planet Earth most of the surface is covered by water. We call it "the blue planet". The ocean is a chaotic system of particles moving and interacting with each other and the surroundings [Vallis 2017b]. In an attempt to understand how nature behaves, it is crucial to understand the ocean, as it is crucial to understand our own world. This is true both out of curiosity but also out of necessity, as we face climate change on our blue planet.

To do this scientists create models. But modelling the world is not an easy task. The complexity and the chaotic nature of the earth system makes it impossible to create a true representation. Ocean General Circulation Models (OGCMs) attempt to picture the large flows and structures, while implementing assumptions on smaller processes. This study focuses on an ocean model with a resolution of 4°x 4°, which means that everything of smaller scale is either neglected or need to be expressed by larger processes.
Mesoscale eddies are a turbulence phenomenon, which are sub-grid scale and as they are important for the overall structure of the ocean, they need to be parametrised [Poulsen 2018][Vallis 2017c]. They could be described as the weather of the ocean and are often pictured as swirls, which can actually be seen from space. In some areas of the ocean eddies are so abundant [Vallis 2017a] calls it "a sea of eddies".
Typically a model needs tuning to match observations from the real world. Tuning is not a sign of a bad model but more a confession stating "this is our best guess" and thus tuning choices must be justified. The tuning process might also reveal limitations and structures of the model [Hourdin et al. 2017]. At the same time one must be aware of the risk of over fitting and keep in mind that tuning might compensate for model deficiencies elsewhere. This study tunes the parametrisation of the eddy kinetic energy (EKE) constructed by [Eden and Greatbatch 2008] using targets of mixed layer depth (MLD) and the strength of the Antarctic Circumpolar Current (ACC).

2 Theory

This section explains the theoretical background for investigating eddy kinetic energy. The goal of this section is to describe how the prognostic EKE-budget is determined and what processes contribute to the formation of eddies. This section will cover Reynolds averaging leading to the closure problem, which the Gent-McWilliams parametrisation is a suggested solution for. The sources and sinks of EKE are analysed to identify the most significant processes.

2.1 Turbulence and the closure problem

The Navier-Stokes equation, governing fluid flows, is highly non-linear. This makes small fluctuations in the system significant. Considering a flow with velocity $\mathbf{u} = (u, v, w)$

decomposed into $\mathbf{u} = \bar{\mathbf{u}} + \mathbf{u}'$. $\bar{\mathbf{u}}$ is the mean velocity, and $\mathbf{u}'$ is a fluctuation, which satisfies $\bar{\mathbf{u}'} = 0$, if averaged in space and time (denoted by the bar). This method is known as Reynolds decomposition. Using this Reynolds decomposed velocity in the Navier-Stokes equation the x-component in the case with constant density results in equation 1 [Vallis 2017b]:

$$\frac{\partial \bar{u}}{\partial t} + (\bar{\mathbf{u}} \cdot \nabla)\bar{u} = -\frac{\partial \bar{p}}{\partial x} + -\nabla \overline{\mathbf{u}' u'} \tag{1}$$

Where $\bar{u}$ is the mean velocity in the x-direction, p, is the pressure, and the last term $\nabla \overline{\mathbf{u}' u'}$ is the Reynolds stress term. Bold font denotes the velocity vector. The velocity profile of the mean flow in the x-direction is dependent on the fluctuations in all directions. The overall problem - the closure problem - is to express these fluctuating parts by the mean variable, as these do not average out because they are non-linear [Brunton 2021]. To simulate the worlds oceans in a coarse resolution model these fluctuations, that we can't simulate, need to be expressed as they have an impact on the overall dynamics of the system.

2.2 Baroclinic instability

Any flow we encounter in nature must be a solution of the Navier-Stokes equation. As described in section 2.1 small fluctuations can have a large influence, meaning that the flow can be unstable. An important mechanism that makes a flow unstable is baroclinic instability. This instability gives rise to large scale and mesoscale circulation [Vallis 2017a] and as we will see in section 2.4 it is important for our parametrisation .

Baroclinic instability originates from the rotation of the earth and the stratification of the watermasses. Considering a system like figure 1, where we have uniformly increasing density with depth and latitude. This system resembles the earth system with high temperature near equator and low temperature in the polar regions. The temperature gradient often results in a pressure gradient, which is then balanced by the coriolis force originating from the rotation of Earth [Vallis 2017a]. This configuration results in thermal wind balance $\frac{\partial u}{\partial z} = \frac{\partial b}{\partial y}$. Here u is the zonal velocity (x-direction), z is the depth coordinate, y meridional coordinate and b is the buoyancy given by $b = -g\frac{\delta\rho}{\rho_0}$, where ρ_0 is a reference density and $\delta\rho$ is the difference from the reference at some point.

Figure 1 shows three fluid parcels in a Boussinesq fluid in geostrophic and hydrostatic balance, meaning that the density variations are small, it is treated as incompressible and the gravitational force is balanced by the vertical pressure gradient. Exchanging two of these water parcels, A and B for example, results in B sinking as it is denser than the surrounding fluid and A rising as it is lighter. This perturbation results in the center of mass for the entire fluid being lowered and thus potential energy is released and converted to kinetic energy. Releasing potential energy from this system results in a restratification as the lowest possible center of mass is when the isopycnals are horizontal.

The Eady problem, which explores baroclinic instability in a simplified system, aims

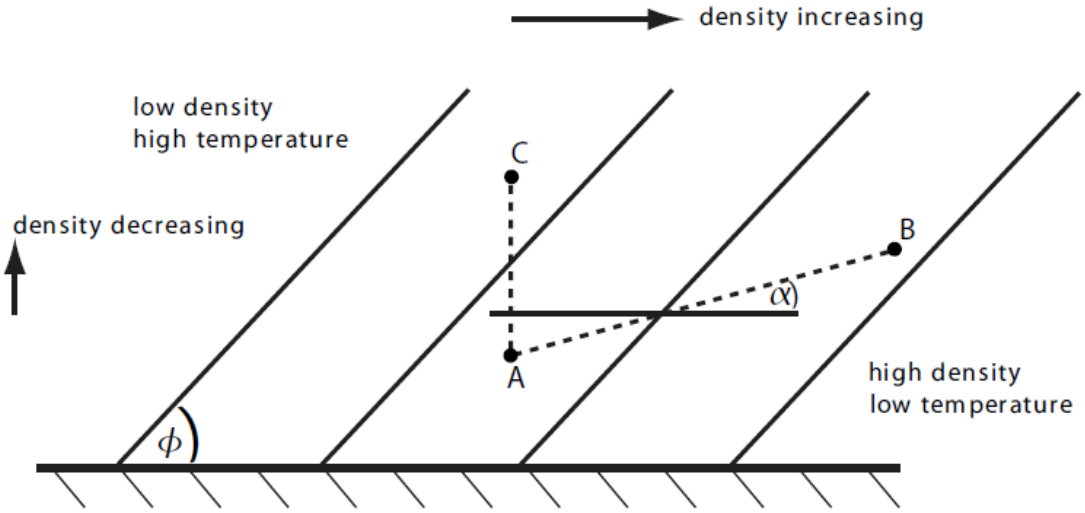

Figure 1: Stratified fluid with densities $C < A < B$, lines with slope ϕ are boundaries of isopycnals. α denotes the slope of the displacement. The relationship $\frac{\alpha}{\phi}$ determines the size of the change in potential energy. Figure taken from [Vallis 2017a]

to explain the stability properties and introduces the deformation length L_d and the Eady growth rate σ_E. The derivation of these will not be covered in detail, but can be found in [Vallis 2017a], the main idea is to begin at the linearized quasi-geostrophic equations and derive an instability criterion which is dependent on the potential vorticity and the mean flow. This analytical solution gives the tools to estimate the size of the instabilities and the timescale in the ocean. The deformation length is on the order of 100 kilometres and the timescale (the inverse of the growth rate) is of about a month [Poulsen 2018]. This gives a rough estimate of the size and life of meso-scale eddies.

In summary, baroclinic instability is a sink of potential energy and flattens isopycnals. The strongest instability occurs on the order of 100 km.

2.3 The Gent-McWilliams parametrisation

In an Ocean General Circulation Model(OGCM) the turbulent mesoscale eddies are typically not resolved. A widely applied method to close this system is the Gent-McWilliams (GM) parametrisation. The goal of the parametrisation is to construct a process flattening the isopycnals while keeping tracers constant between these [Vallis 2017d]. This is also called thickness diffusivity, as the volume of fluid is a conserved quantity and not mixed across isopycnals. It is believed that this parametrisation works for meso-scale eddies as they are driven by baroclinic instability.

Gent and McWilliams use near downgradient Fickean diffusion to close the system [Gent et al. 1995]. Going back to section 2.1 where $\overline{\mathbf{u}}$ is the mean flow velocity and $\mathbf{u}' = (\mathbf{u}'_\mathbf{h}, w')$ is the eddy induced transport velocity. The fluctuations are parametrised

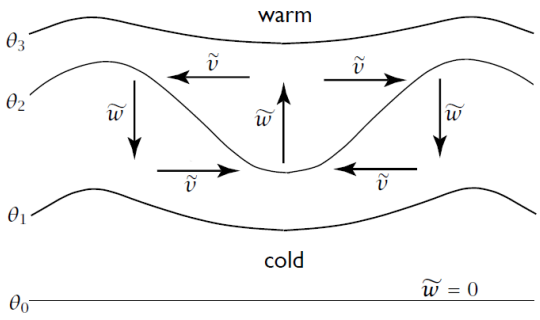

Figure 2: The figure shows the effect of the GM-parametrisation. Lines denoted by θ are isopycnal lines, $\tilde{v}$ is the horizontal velocity and $\tilde{w}$ is the vertical velocity. The figure is found in [Vallis 2017d] p. 439

as:

$$\mathbf{u}'_{\mathbf{h}} = -\frac{\partial}{\partial z} K_{gm} \mathbf{L} \tag{2a}$$

$$w' = \nabla \cdot K_{gm} \mathbf{L} \tag{2b}$$

Here K_{gm} is the thickness diffusivity and $\mathbf{L} = \frac{\nabla \rho}{\frac{\partial}{\partial z}\rho}$ [Gent et al. 1995]. Gent and McWilliams introduce this diffusivity as a scalar on the order of $o(10^3 \frac{m^2}{s})$ [Eden and Greatbatch 2008].

The effect as shown in figure 2 is a rotation of the fluid minimizing the potential energy. The interesting mechanism of the GM-parametrisation is that the horizontal diffusion is directed downgradient while the vertical is upgradient. The resulting skew flux is directed along the isopycnals.

In [Eden and Greatbatch 2008] the GM-parametrisation is used on the horizontal and vertical buoyancy fluxes, they write these as:

$$\overline{\mathbf{u}'_h b'} = -K_{gm} \nabla_h \bar{b} \tag{3a}$$

$$\overline{w' b'} = K_{gm} \frac{|\nabla_h \bar{b}|^2}{N^2} \tag{3b}$$

Here b' is a small fluctuation in buoyancy, $\bar{b}$, K_{gm} is the thickness diffusivity which needs to be determined and $N^2 = \frac{-g}{\rho_0} \frac{\partial \rho}{\partial z}$ is the buoyancy frequency which is defined by the density of the fluid parcel and describes the stratification [Mrozowska 2024].

Building on observations Eden and Greatbatch argues that K_{gm} varies spatially. Using the GM-parametrisation and a mixing length approach they assume [Eden and Greatbatch 2008]:

$$K_{gm} = LU \tag{4}$$

Where L and U are a characteristic eddy length scale and velocity. U is defined by the eddy kinetic energy, $U = \sqrt{\bar{e}}$.

In summary the GM-parametrisation serves the purpose of lowering the potential energy by redistributing fluid like baroclinic instability. This closure can be numerically integrated in an eddy kinetic energy budget.

2.4 The eddy kinetic energy budget

The prognostic eddy kinetic energy (EKE) budget, constructed by Eden and Greatbatch in their paper 'Towards a mesoscale eddy closure' [Eden and Greatbatch 2008], is used in Veros (sec: 4.1). This equation originates from applying assumptions to the governing EKE budget. Eden and Greatbatch identifies this as:

$$\frac{\partial}{\partial t}\bar{e} + \bar{\mathbf{u}} \cdot \nabla \bar{e} = \bar{S} + \overline{b'w'} - \epsilon - \nabla \cdot \mathbf{M} \tag{5}$$

The following description aims to compare this governing EKE budget (eq. 5) to the numerical scheme used to calculate EKE as a model equation. These correspond to equations 6 and 27 in [Eden and Greatbatch 2008].

The right hand side of equation 5 contains $\bar{S}$, which describes eddy momentum fluxes and the exchange of energy with the mean flow. The term $\overline{b'w'}$ describes energy production due to baroclinic instability, ϵ is the dissipation of energy and the last term which is of advective nature, relate fluctuations of the mean flow and pressure to the EKE: $\nabla \cdot \mathbf{M} = \nabla \cdot \overline{\mathbf{u}'e} + \nabla \cdot \overline{u'p'}$

Eden and Greatbatch characterize these using four headlines: Energy production related to eddy momentum fluxes, Energy production related to baroclinic instability, Dissipation and Radiation. Each contain fluctuations that needs to be parametrised, this is done with the GM-parametrisation.

The resulting prognostic EKE budget which can be integrated in Veros is then:

$$\frac{d}{dt}\bar{e} = K_{gm}|\nabla_h \bar{u}|^2 + K_{gm}\frac{|\nabla_h \bar{b}|^2}{N^2} + \frac{f^2}{N^2}\frac{\partial K_{gm}}{\partial z}\frac{\partial \bar{E}}{\partial z} + \nabla_h \cdot K_{gm}\nabla_h \bar{e} + \frac{\partial}{\partial z}\left(0.1K_{gm}\frac{f^2}{N^2}\frac{\partial \bar{e}}{\partial z}\right) - c_\epsilon \frac{\bar{e}^{\frac{3}{2}}}{L} \tag{6}$$

The right hand side of equation 6 contains six terms controlling the change in EKE over time which is the left hand side. Here K is scaled by c_k which is a tuning parameter, $K_{gm} = c_k L\sqrt{\bar{e}}$. f is the Coriolis frequency, N^2 the buoyancy frequency, $\bar{E}$ is the average energy of the mean flow and L is a characteristic length scale. This is chosen as the minimum of the Rhines length and the Rossby length [Eden and Greatbatch 2008]
Comparing equation 5 with equation 6 we have:

$$\bar{S} = K|\nabla_h \bar{u}|^2 + \frac{f^2}{N^2}\frac{\partial K}{\partial z}\frac{\partial \bar{E}}{\partial z} \tag{7}$$

$$\overline{b'w'} = K\frac{|\nabla_h \bar{b}|^2}{N^2} \tag{8}$$

$$\nabla \cdot M = -\nabla_h \cdot K \nabla_h \bar{e} - \frac{\partial}{\partial z}\left(0.1K \frac{f^2}{N^2}\frac{\partial \bar{e}}{\partial z}\right) \tag{9}$$

$$\epsilon = c_\epsilon \frac{\bar{e}^{\frac{3}{2}}}{L} \tag{10}$$

Equation 7 is related to transfer of energy specifically diffusion of mean relative vorticity. This originates from the assumption that potential vorticity is mixed downgradient of mean potential vorticity and not momentum itself. It is also assumed that the diffusivities are identical for all terms. Eden and Greatbatch note that this might not hold in reality, but it ensures that both potential vorticity and buoyancy is mixed downgradient [Eden and Greatbatch 2008].
Obtaining an expression for $\bar{S}$ is done by computing the change in EKE from the Mean Kinetic Energy (MKE) budget. What kinetic energy is lost in the mean flow is transformed to EKE.
The first term, in eq. 7 is the horizontal shear of the mean flow, the second is the vertical derivative of the thickness diffusivity which is found through the derivation to be related to the stretching vorticity.

Equation 8 is the assumed down gradient diffusion of buoyancy, which is related to baroclinic instability. Equation 9 consists of isotropic mixing of EKE by the first term and the second term is the vertical mixing of EKE. Equation 10 is the dissipation to smaller scales and this is tuned by the parameter c_ϵ. Note the sign on equations 9 and 10.

To find how the relative sizes of the sinks and sources of this equation, each term is plotted in figure 3. They are evaluated along a line in the Pacific ocean to analyse the structure of this equation in the ocean. The method is inspired by [Jochum, Malanotte-Rizzoli, and Busalacchi 2004]
A line between 50°N and 50°S at 170° W is chosen. To minimize grid noise the values are zonally averaged between 160° and 180° West, refer to figure 10 in the appendix. To compute each term, model output from the default Veros setup (see section 4.1) is used to calculate the values. For gradients a first order numerical differentiation scheme is used for the calculation.

In figure 3 we see a clear difference between the different depths with the vertical mixing of EKE being dominant near the surface in the southern ocean, the terms are approximately the same size elsewhere. In figure 3b it is visible that the baroclinic instability term dominates in the southern ocean along with the vertical derivative of thickness diffusivity. This is consistent with what is found in [Eden and Greatbatch 2008] for the interior ocean. Furthermore figure 3b shows that the dissipation balance out the production.

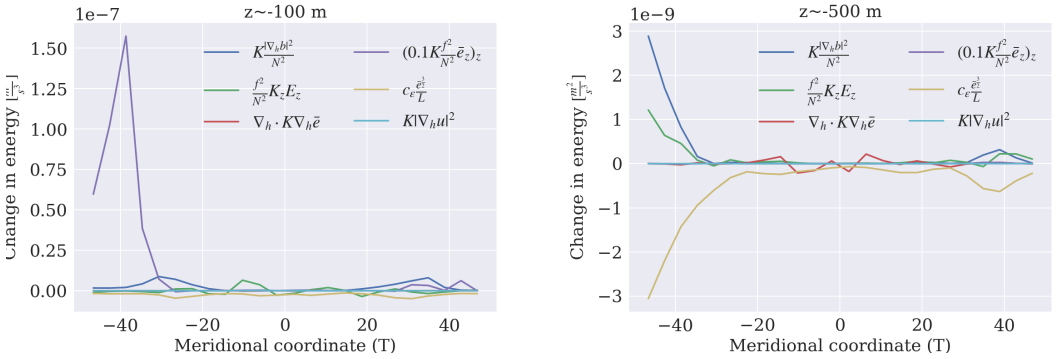

(a) Size of each term at 100 m depth.

(b) Size of each term at 500 m depth.

Figure 3: Scale analysis of the EKE budget. Note that the y-axis scales by 10^{-7} for 100m and 10^{-9} for 500 m.

3 Data

In this project observational data is used as a target for the optimization of parameters. The targets are the Mixed Layer Depth (MLD) and the strength of the Antarctic Circumpolar Current (ACC). The first is chosen as ocean models show large biases towards mixed layer depth in the southern ocean Mrozowska 2024. The mixed layer depth is often defined by a thresh hold:

$$\rho(MLD) = \rho(z_{ref}) + \delta\rho \tag{11}$$

Simply put, to find the mixed layer depth at some place in the ocean, the density is measured at the reference depth. then the mixed layer depth is found by increasing the depth until the density thresh hold is found.

This project uses the dataset [Boyer Montégut 2022] which originates from the ARGO program. The dataset has a reference depth of $z_{ref} = 10$ meters and $\delta\rho = 0.03\frac{kg}{m^3}$ [Boyer Montégut 2022]. Thus the mixed layer depth is a measure for the thickness of the isopycnal layer at 10 meter depth, which makes it well suited for exploring the effect of the parametrisation of thickness diffusivity. The dataset is constructed from 7.3 million measurements of temperature and salinity made at sea between 1970 and 2021 using eq. 11. The same criterion is used in Veros to comapare the MLD.

The second target for the optimization process is the strength of the ACC. In this project a value of 137 Sverdrups is chosen as target following [Cunningham et al. 2003]

4 Method

In this section the ocean model used for optimization and the optimizing tool is explained. Furthermore the initial considerations regarding the model and the optimization of the EKE-budget is briefly noted.

4.1 Veros

The ocean model Veros (Versatile ocean simulator) is optimized in this project. Veros uses explicit time stepping to integrate primitive equations under semi-compressible, hydrostatic and Boussineq approximations [Häfner, Nuterman, and Jochum 2021]. These equations are numerically solved on a staggered Arakawa-C grid where all variables, tracers and fluxes are calculated on different grid points. In this project a 4 degree model is used. This model has 60 (z) vertical layers 40 (y) meridional layers and 90 (x) zonal layers making a grid cell at the equator about (440 x 440) km (using $1^\circ \approx 110$ km). The vertical spacing increases towards the bottom and the top layer is 4 meters. The relative coarseness of the model has the advantage faster computation. A model year can be computed in 2.8 minutes, while increasing the resolution to 1° x 1° results in 8 hours of computation per model year on the Aegir cluster [Mrozowska 2024] [Häfner, Nuterman, and Jochum 2021]. This is a coarse model setup as processes on the mesoscale and smaller are not resolved. The horizontal resolution is much larger than the eddies (section 2.2) and the parametrisation from section 2.4 is used in Veros.

4.2 Veropt and Bayesian optimization

Often in climate modelling parameters need to be tuned to make the model fit data or for the model to make sense physically. It is meaningful to ask how these parameters should be chosen as one often have to compromise between targets and 'choosing' a value can seem rather subjective.

To tune the EKE parameters c_k and c_ϵ this project uses the Bayesian Optimizing (BO) tool Veropt, which was developed specifically for optimizing Veros parameters by Stoustrup 2024. An attempt to optimize the turbulent kinetic energy closure has already been made in [Mrozowska 2024] "Fast and Efficient: Bayesian Optimization with GPU Acceleration for Ocean Models".

As [Stoustrup 2024] write in their thesis about the construction of Veropt the expected number of simulations are around the order of 100. Often times one would choose on the order of millions, but in ocean modelling the time and computational cost limits this approach [Mrozowska 2024]. What Veropt essentially does is to make 'clever' guesses about where optimal parameters could be located.

To explain Veropt, it is useful to examine figure 4.

Going through the figure, first step is to pick a kernel. The Matérn kernel is default in Veros and also what is used in this project. The kernel could be specified if we had an idea of how the objective function could look. Kernel choice is beyond the scope of this project

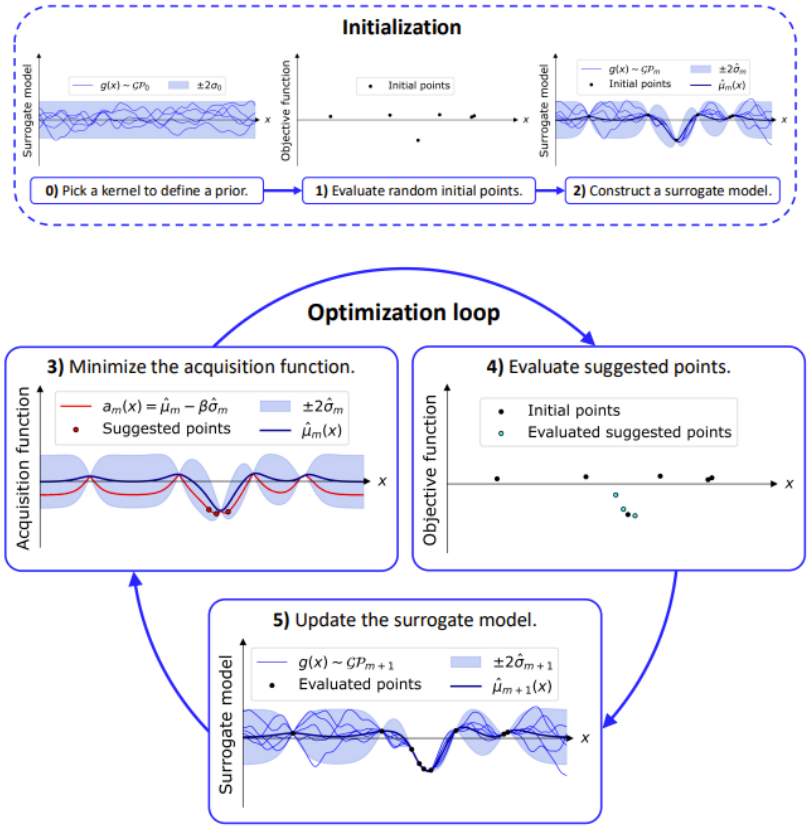

Figure 4: This figure is taken from [Mrozowska 2024]. It displays a one dimensional example of a Gaussian process.

The optimization process begins by choosing random initial points. In this project random parameters of c_k and c_ϵ within some boundaries are used in a simulation and the value of the objective function which is the combined error to the targets are these points. From these values the surrogate model is constructed.

In the optimization loop the acquisition function (eq. 12) is minimized to determine which objective function points to evaluate next. The acquisition function is calculated from the constructed surrogate model:

$$a(\bar{x}) = \hat{\mu}(\bar{x}) - \hat{\sigma}(\bar{x})\beta - r\hat{\sigma}(\bar{x})\beta\gamma \tag{12}$$

This equation consists of the mean ($\hat{\mu}$) of the surrogate model constructed from the objective function. The second term ensures that areas with large uncertainty given by the standard deviation $\hat{\sigma}$ influence the picking of new points. One could imagine a point with a large uncertainty could in fact be an extrema. The last term in the acquisition function serves the purpose of adding some noise to a point in the case that the objective function is nearly constant along a parameter.This ensures that the optimization process keeps exploring the structure of the objective function. For each round in the optimization loop more and more objective function values are evaluated and the extrema is located.

The process is used in this project to tune c_k and c_ϵ from section 2.4.

Stoustrup describes the relation between these terms as "exploration vs exploitation" [Stoustrup 2024] by choosing a β we can force the tool to search near extremas we have already found or search areas with larger uncertainty.

4.3 Experimental setup and initial investigation

In this study two experiments are conducted using different latitude ranges of the MLD dataset. One uses the range 60°South to 30°North to focus on the southern ocean bias, this will be named MLD-60S30N. The other is symmetric about the equator in the range 50°South to 50°North and will be named MLD-50S50N.
Different ranges are used to see if the optimal parameters are reproduced and how the structure of MLD, the impact on K_{gm}, ACC strength and the AMOC differs between the experiments.

Before conducting the experiment and optimizing the parameters with observational data, the spinup of the relevant processes are checked. These being the ACC strength, the MLD, and the strength of the Atlantic Meridional Overturning Circulation (AMOC). Ensuring the spin up is important as we need to compare these modelled values with observations. These are shown in the appendix at figures 13, 14 and 15. It is estimated that the ACC is the last of these processes to spin up and that it takes approximately 80 model years.

Optimizing the parameters has influence on various other processes. In this project the AMOC is evaluated and analysed for these parameters to see how this is affected.

Furthermore the sensitivity of the vertical spacing of grid points are checked. It is an important question to ask if the interpolation between points makes a considerable difference in the calculation of MLD.
Simulations with a varying number of layers (figure 17 in the appendix) show that the mixed layer is approximately the same in the mid-latitude while differences arise around 60 degrees south. This is likely due to difficulties in calculating the MLD in high-latitude regions. The optimization will focus on the mid-latitude region.

To get an initial idea of the response of the model to the parameters c_k and c_ϵ, an experiment with default values for MLD and ACC strength as a target was conducted. The resulting parameter space of the optimisation can be seen in the appendix in figure 18.

The initial experiment serves a number of purposes. First of all I wish to confirm the methods ability to find a predetermined optimal parameter set for the EKE. This has already been done by optimizing the MLD in a twin experiment with the Turbulent

Kinetic Energy (TKE) [Mrozowska 2024].

In this project the EKE is optimized with two targets, which is slightly different, compared to [Mrozowska 2024], in the way that the objective function value is the average of these two errors. They are weighted equally and optimized simultaneously. The experiment is done to confirm that the method is valid for optimizing multiple parameters to multiple targets, by the method described in the section 4.2.

An equally important focus is trying to determine the sensitivity of each of these errors due to the parameters. These are found to be on the same order of magnitude, with MLD error being sligthly larger. The weight of each could be chosen differently but are kept for this reason.
Exploring the errors in this parameter space also gives an indication of a relation between the parameters as Mrozowska found considering TKE [Mrozowska 2024]. Obtaining the error for both MLD and ACC strength shows that parameters minimizing error for one target enlarge errors for the other.

5 Results

5.1 Observational experiments

With the data described in section 3, the optimizer produces the parameter spaces shown in figure 5. The figure shows the default parameter set with an X and the optimal parameter set with a +.

The optimal parameter sets and their errors are shown in table 1.

	MLD - 30N60S	MLD - 50N50S	Default
c_k	10.0	0.28	0.5
c_ϵ	20.0	0.0025	0.4
c_k/c_ϵ	0.5	112.4	1.25
MLD (RMSRE)	0.53	0.43	1.1
ACC strength (RE)	-0.35	-0.31	-0.23
Objective function error	0.44	0.36	0.67

Table 1: The optimized parameters with their errors. RMSRE is root mean square relative error, RE is relative error. The error on MLD is calculated for their respective latitude ranges, while the error on the default is on the entire range from 50°N to 60°S.

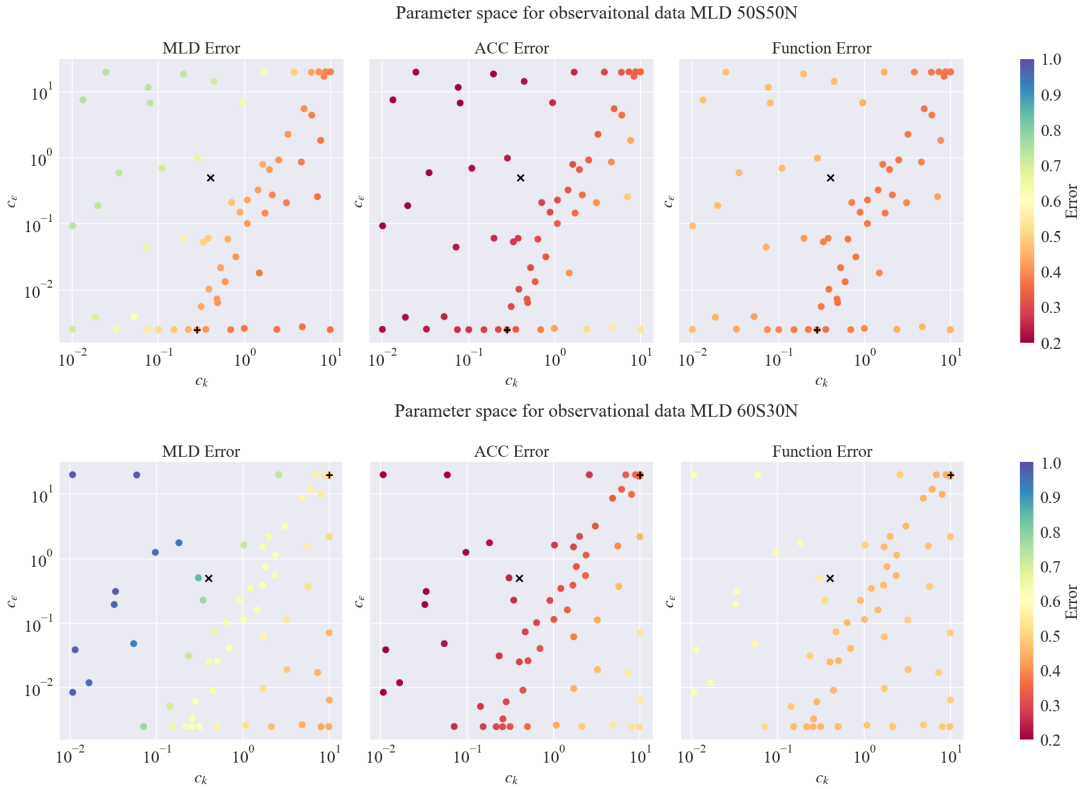

Figure 5: Parameter space for experiments: Points show a set of parameters in (c_k, c_ϵ) space. The color of the point denotes the calculated error. The error of the objective function is the average of the absolute errors on MLD and ACC strength. On each figure the default and the best parameter set are plotted.

6 Discussion

6.1 The parameter space

Examining figure 5 the parameter spaces for both experiments are shown. The error is shown on the colorbar, for MLD, ACC strength and objective function. As explained in section 4.2 Veropt minimizes the error on the objective function, which is the combined errors on MLD and ACC strength. From this plot it is clear, that the error on MLD is more dominant than the ACC strength as the errors are larger on the MLD in both experiments. For MLD-50S50N the MLD error ranges between 0.4 and 0.8 while the ACC error lies between 0.2 and 0.6. The same is true for MLD-60S30N with MLD errors between 0.45 and 1.0.

It is apparent that the error on MLD is larger when the southern ocean is favoured, which also increase the error on the objective function. This can be seen as all points have a larger error relative to the MLD-50S50N experiment. In figure 5 the error for MLD-60S30N is 0.53 while it is 0.43 for the symmetric experiment on the optimal parameter sets. The same pattern is seen for all other points with the objective function error being

larger in MLD-60S30N by between 0.1 and 0.2. By choosing the target region the error is changed.

Comparing the experiments with a default simulation in table 1 it is seen that the optimal parameters differs by several orders of magnitude and that neither of the experiments produce the default parameters. The largest difference lies in the dissipation.

The experiments show the same tendency for the parameters. There appears to be a ridge of optimal parameters that vary little in error magnitude. This ridge could be interpreted as an optimal relation between c_k and c_ϵ where these tuning parameters ensure an optimal level of EKE.
As covered in section 2.4 c_k controls the production and c_ϵ the dissipation, meaning that the relative sizes of c_k and c_ϵ is the important factor of controlling EKE. This would correspond to the result found in [Mrozowska 2024], where TKE was examined.

From figure 5 it is seen that minimizing the error on one of the targets enhances the error on the other. This makes the lowest error on the objective function a compromise between the two and thus a global maximum isn't found by the optimization, but a ridge is.
This understanding reveals that our targets counteract each other and that tuning the EKE-budget-parameters might not be able to embrace both.

6.2 Impact on model output

To evaluate the optimized parameters for each experiment the various variables for the different simulations are plotted. In this project the focus is on K_{gm} which as covered in the theory section is scaled by c_k, and the EKE itself which is a model output. Furthermore the MLD and the strength of the ACC, which are both targets, are analysed for the optimized parameters. Figure 6 show these compared to the default Veros simulation and the target dataset. Figure 8 shows K_{gm} and EKE.

In figure 6a, approximately the same mixed layer depth are found for both optimization experiments around the equator. Differences arise around 35°South. It is clearly visible that all models deviate from the observations going towards the poles. The figure also shows the southern ocean bias in the default model towards a deeper mixed layer compared to observations.

In this project it is chosen to zonally average the mixed layer depth, as differences are more easily recognized than on a longitude/latitude map. A comparison map is shown in the appendix, figure 12.

Figure 6b shows the ACC strength. The transport can also be plotted on a map and

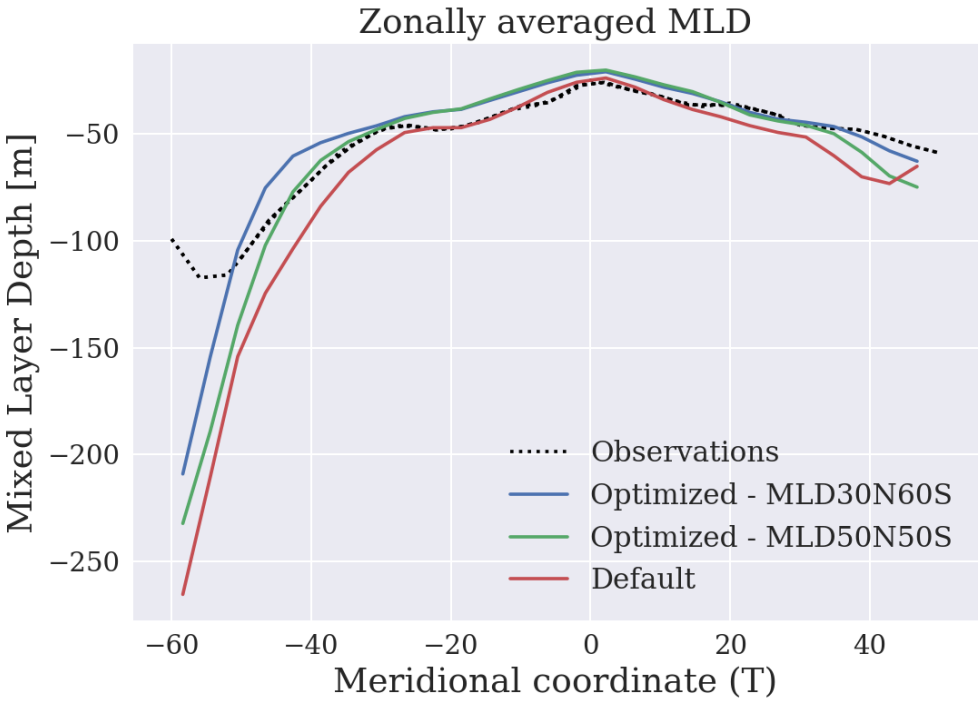

(a) Zonally averaged mixed layer depth for the optimized parameters and for the default parameters, with the observations serving as the target for the Bayesian optimization.

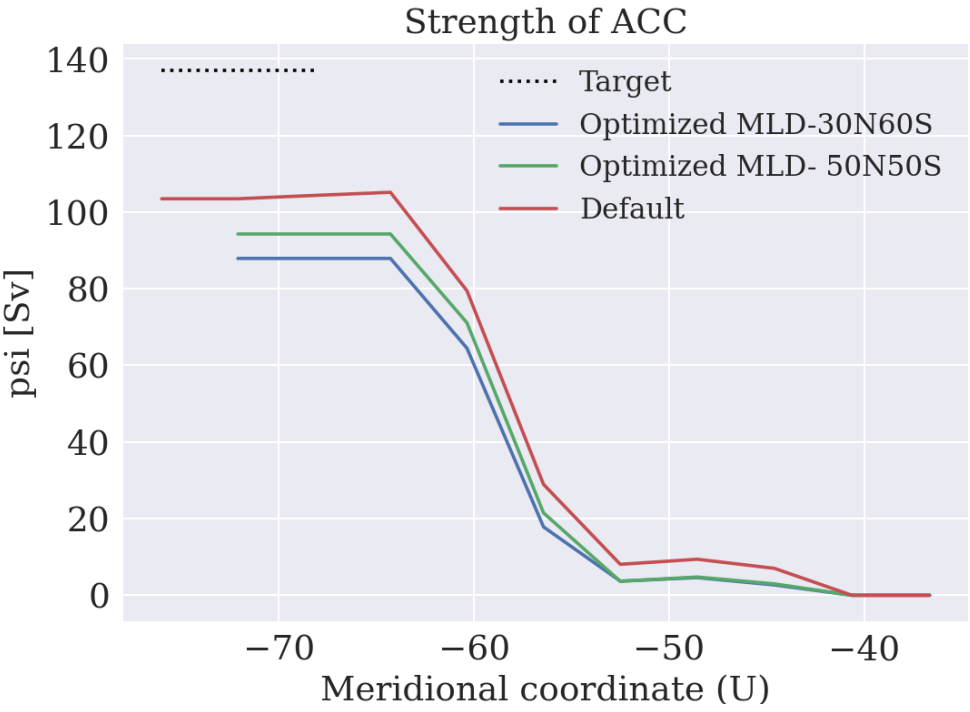

(b) Maximum transport of the ACC in Sverdrups at Drakes Passage.

Figure 6: Comparison of zonally averaged mixed layer depth (top) and ACC transport strength (bottom) for the optimized and default parameters.

compared to the default Veros output. This is shown in figure 7. From these figures it is visible that the ACC transport is weaker in MLD-30N60S than in the symmetric experiment. An interesting aspect to note is that the Gulf stream has approximately the same magnitude in both experiments.

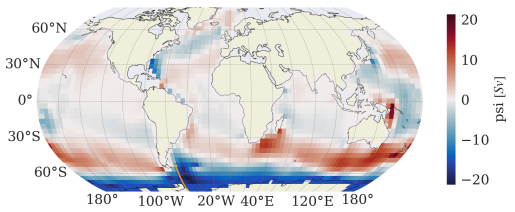

(a) MLD-30°N 60°S relative transport to default (optimized - default)

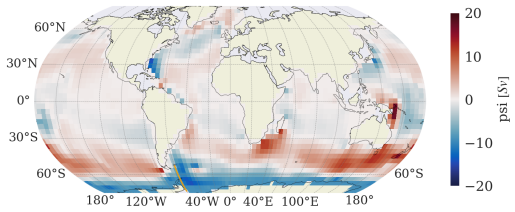

(b) MLD-50°N 50°S relative transport to default (optimized - default)

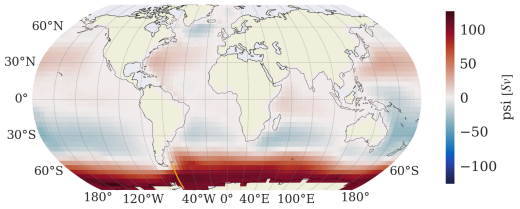

(c) Default transport

Figure 7: The transport in Sverdrups compared to the default for both experiments. The orange line corresponds to where the target value is compared to the optimized. The maximum is found along the line

Looking at K_{gm} and EKE in figure 8 zonally averaging is chosen as the preferred method to display these results. This is done because the structure in the vertical coordinate is interesting. In the appendix a figure showing the EKE at 1000 meters depth can be found (figure 11). This figure shows how the EKE , zonally, is the same order of magnitude in the same region as the ACC, which indicates that the zonal average is acceptable focusing on the southern ocean.

Figure 8 reveals that a large thickness diffusivity doesn't necessarily result in a large amount of EKE. The sources of EKE (see section 2.4), which is scaled by K_{gm}, is balanced by the dissipation. Thus it could be argued that the relative size of c_k and c_ϵ does control the size of EKE.

The optimal level of EKE discussed above is different for the experiments as figure 8b clearly shows. The optimized parameters result in EKE-levels that differ by 4 orders of magnitude, while they maintain the same structure.

One would expect a larger amount of EKE would result in a weaker ACC. Looking at the region 60°S to 30 °south and comparing this area with figure 7, it is true that the

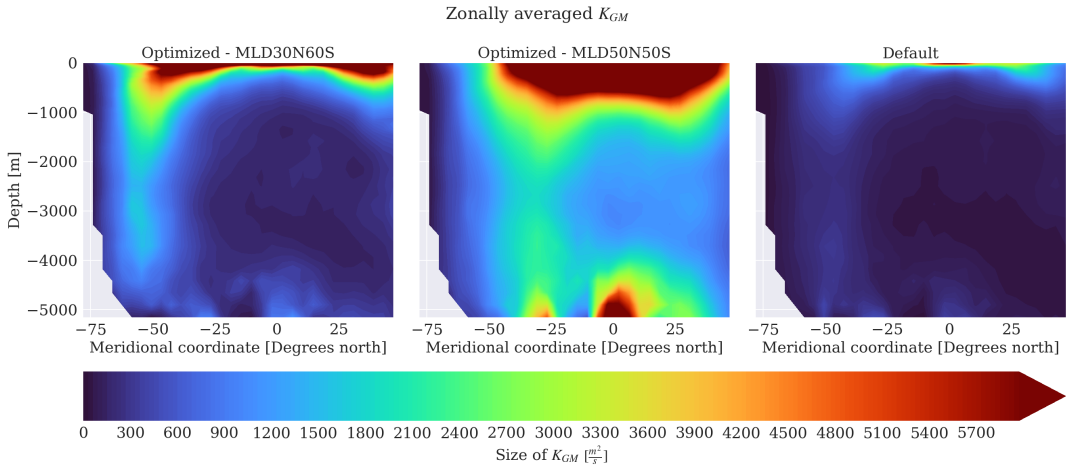

(a) Size of K_{GM}, values are as high as 10^3, but these are not included to show the structure in the interior.

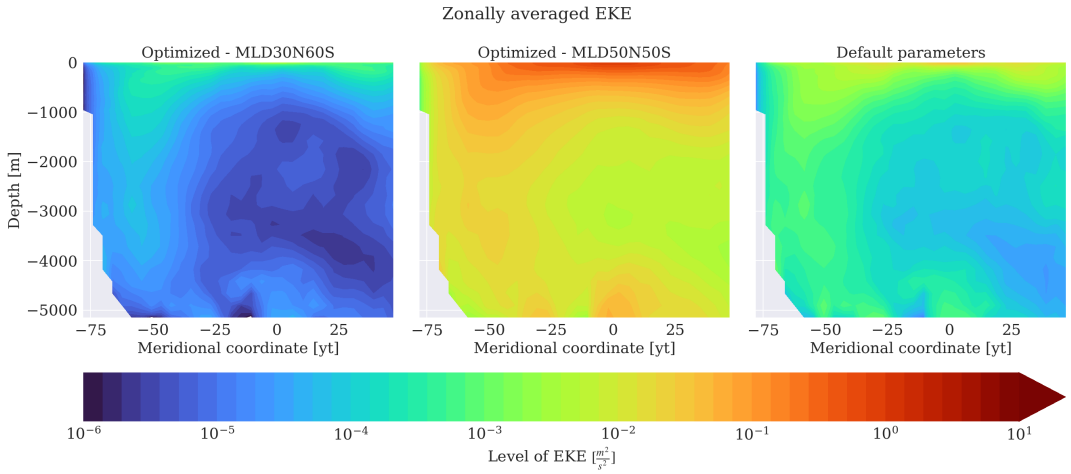

(b) Size EKE for each experiment.

Figure 8: Model output for optimized parameters and default.

ACC is weakened concerning the MLD - 50N50S experiment but surprisingly a smaller amount (compared to default) of EKE, which is the result of MLD - 30N60S, also weakens the ACC and by an even greater amount. The connection between the weakening of the ACC and EKE lies in the transfer of kinetic energy from the mean flow to EKE. This effect is seen in figure 8a as K_{gm} controls this effect. In section 2.4 this energy transfer is related to $\bar{S}$.

Concerning section 2.2 one would expect potential energy to be converted to EKE by baroclinic instability. This is a direct cause of the flattening of isopycnals that the thickness diffusivity accounts for. This effect is seen in figure 6a and most clearly in the region 35°south to 55°south where the simulations differ. Comparing this to figure 8a we see that K_{gm} is concentrated more to the south for MLD-60S30N than MLD-50S50N, flattening isopycnals more in this region.

One could interpret this result as K_{gm} being the driver of flattening isopycnals, creat-

	MLD - 30N60S	MLD - 50N50S	Default
$K_{gm}(\frac{m^2}{s})$	2000	2700	600
EKE $(\frac{m^2}{s^2})$	10^{-4}	$5 \cdot 10^{-2}$	10^{-3}
ACC (Sverdrups)	88	94	104
c_k/c_ϵ	0.5	112.4	1.25

Table 2: Characteristic values for the model output in the different simulations.

ing EKE but given the large dissipation, in the MLD-30N60S experiment, the energy is transferred to smaller scales. This interpretation is supported by the fact that the regions with large K_{gm} are different for the optimized parameters.
In MLD-30N60S the thickness diffusivity is primarily focused between 60°S and 50°S, where in contrast it is located around 30°S in the other experiment.
This is most likely a result of the target dataset of MLD. Looking again at figure 6a, it is seen that this happens at the cost of a shallower MLD in the tropic region. This interpretation is also valid for the default parameters as a large deviation from the observations is seen in the Southern Ocean, corresponding to low values of K_{gm}.

Collecting the information for the three regimes (the two experiments and the default), the following numbers paints the picture. For MLD-60S30N at about 55°south at 2000 m depth $K_{gm} \approx 2000\frac{m^2}{s}$, this results in an EKE in the same area of $\approx 10^{-4}\frac{m^2}{s^2}$ these values result in an ACC transport at 88 Sverdrups. For MLD-50S50N the structure is slightly "shifted" towards equator as explained, but at 2000 meters at 35°south $K_{gm} \approx 2700\frac{m^2}{s}$ and EKE $\approx 5 \cdot 10^{-2}\frac{m^2}{s^2}$ resulting in a transport of 94 Sv.

Table 2 shows these values and $\frac{c_k}{c_\epsilon}$. It could be argued that the slowing of the ACC is due to a large K_{gm}, while the relationship of c_k and c_ϵ controls the EKE-level.

This analysis show that the optimization depends on the targets chosen. First of all the parameter space showed that the individual targets preferred different regions of the parameter space and second that the experiments yielded two very different optimal parameter sets. Secondly vastly different parameters result in different levels of EKE that optimize the MLD in different regions. This project shows that even when one tries to objectively tune parameters subjective choices are made.

6.3 The rest of the world

So far the focus has mainly been on the targets of the optimizer and the direct effect on the EKE-budget. Another important aspect is how this optimization affects the rest of the model. It is an important question to ask if the optimal parameters are optimal across the model and how it affects other dynamics.
With many simulations conducted a relation between the strength of the ACC and the AMOC can be constructed.

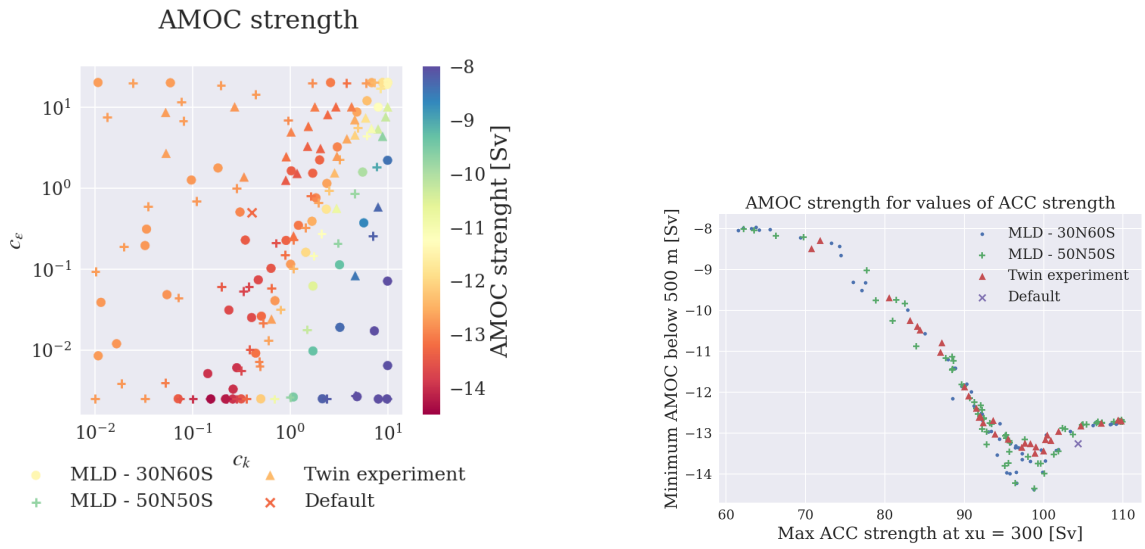

(a) AMOC strength parameter space.

(b) AMOC vs ACC.

Figure 9: Comparison of AMOC strength in parameter space and its relationship with ACC.

Figure 9b shows how the strength of the ACC and the AMOC is related. The AMOC strength is the maximal southward meridional transport below 500 meters at 24°N. An example of this value can be seen in appendix 16 It is clearly seen that the strength of the ACC and of the AMOC is correlated. It is not possible though, to determine if there is a causal link between the two, as there could be many reasons for these to be related. Figure 9a shows a clear tendency favouring low values of c_ϵ, when maximizing the southward AMOC transport. Further figure 9a shows that the AMOC strength is maximized in the same region as the optimal parameters for MLD-50N50S. Optimizing with AMOC strength as an additional target could be a future project.

6.4 Improvements and future work

In this optimization process all grid points are weighed equally for the MLD. But as the grid size gets smaller closer to the poles the density of grid points increases. This means essentially that a smaller area close to the poles is overrepresented compared to an area near the equator. One could chose to weigh the error by grid size and thus eliminate this aspect. This would serve the purpose of optimizing everywhere, but again as described in the previous section the optimization is highly dependent on the target chosen.

To determine if either one of the optimized parameter sets in this project is to be preferred one could further examine and validate other model output. This could be the strength of the Gulf stream or temperature gradients. As explained earlier the large difference in EKE which may be a result of the dissipation could be tracked and checked.

Other processes in Veros could also have influence on the MLD and ACC strength. Wind stress is usually tuned as [Poulsen 2018] does. The MLD is affected by other mixing processes in the ocean and is also influenced by the turbulent mixing as shown in [Mrozowska 2024]. Meso-scale eddies and turbulent kinetic energy aren't the only processes of turbulent mixing occurring in the ocean. In [Eden, Czeschel, and Olbers 2014] the authors closes the energy cycle combining turbulent closures. Optimizing and analysing such a system could potentially reveal more about how EKE affects the model.

7 Conclusion

The optimization of the parameters c_k and c_ϵ in the EKE budget results in $c_k = 10.0$ and $c_\epsilon = 20.0$ with an error of 0.44 when optimized to an MLD dataset extending from 60°south to 30°north. A similar optimization in the range 50°south to 50°north results in $c_k = 0.28$ and $c_\epsilon = 0.0025$ with 0.36. Both simulations uses an ACC strength of 137 as additional target.

The analysis of model output shows that there are different optimal levels of EKE as these differs between the experiments by two orders of magnitude. The analysis showed that the slowing of the ACC is due to a large K_{gm}, and the relationship of c_k and c_ϵ is the important factor controlling the EKE-level. This project shows that objective tuning of parameters depends on the choice of targets and that the tuning of these parameters doesn't eliminate the MLD bias everywhere. In this project the optimal parameters become a compromise between the MLD and ACC error as they are minimized in different regions of the parameter space.

Thereby it can be concluded that the processes concerning MLD and ACC strength is not entirely described or captured by the parametrisation used in this coarse resolution model.

8 Literature

References

Boyer Montégut, C de (2022). "Mixed layer depth climatology computed with a density threshold criterion of 0.03 kg/m3 from 10 m depth value". In: SEANOE [data set] 10, p. 91774.

Brunton, Steven L. (Apr. 2021). Turbulence: Reynolds Averaged Navier Stokes (RANS) Equations (Part 2, Momentum Equation). Data Driven Fluid Dynamics. Accessed: 2025-01-02. DOI: 10.52843/cassyni.1xkvn0. URL: https://doi.org/10.52843/cassyni.1xkvn0.

Cunningham, S. A. et al. (2003). "Transport and variability of the Antarctic Circumpolar Current in Drake Passage". In: Journal of Geophysical Research: Oceans 108.C5. DOI: https://doi.org/10.1029/2001JC001147. eprint: https://agupubs.onlinelibrary.wiley.com/doi/pdf/10.1029/2001JC001147. URL: https://agupubs.onlinelibrary.wiley.com/doi/abs/10.1029/2001JC001147.

Eden, Carsten, Lars Czeschel, and Dirk Olbers (2014). "Toward Energetically Consistent Ocean Models". In: Journal of Physical Oceanography 44.12, pp. 3160–3184. DOI: 10.1175/JPO-D-13-0260.1. URL: https://journals.ametsoc.org/view/journals/phoc/44/12/jpo-d-13-0260.1.xml.

Eden, Carsten and Richard J. Greatbatch (2008). "Towards a mesoscale eddy closure". In: Ocean Modelling 20.3, pp. 223–239. ISSN: 1463-5003. DOI: https://doi.org/10.1016/j.ocemod.2007.09.002. URL: https://www.sciencedirect.com/science/article/pii/S1463500307001163.

Gent, Peter R. et al. (1995). "Parameterizing Eddy-Induced Tracer Transports in Ocean Circulation Models". In: Journal of Physical Oceanography 25.4, pp. 463–474. DOI: 10.1175/1520-0485(1995)025<0463:PEITTI>2.0.CO;2. URL: https://journals.ametsoc.org/view/journals/phoc/25/4/1520-0485_1995_025_0463_peitti_2_0_co_2.xml.

Häfner, Dion, Roman Nuterman, and Markus Jochum (2021). "Fast, Cheap, and Turbulent—Global Ocean Modeling With GPU Acceleration in Python". In: Journal of Advances in Modeling Earth Systems 13.12. e2021MS002717 2021MS002717, e2021MS002717. DOI: https://doi.org/10.1029/2021MS002717. eprint: https://agupubs.onlinelibrary.wiley.com/doi/pdf/10.1029/2021MS002717. URL: https://agupubs.onlinelibrary.wiley.com/doi/abs/10.1029/2021MS002717.

Hourdin, Frédéric et al. (2017). "The Art and Science of Climate Model Tuning". In: Bulletin of the American Meteorological Society 98.3, pp. 589–602. DOI: 10.1175/BAMS-D-15-00135.1. URL: https://journals.ametsoc.org/view/journals/bams/98/3/bams-d-15-00135.1.xml.

Jochum, Markus, Paola Malanotte-Rizzoli, and Antonio Busalacchi (2004). "Tropical instability waves in the Atlantic Ocean". In: Ocean Modelling 7.1, pp. 145–163. ISSN: 1463-5003. DOI: https://doi.org/10.1016/S1463-5003(03)00042-8. URL: https://www.sciencedirect.com/science/article/pii/S1463500303000428.

Mrozowska, Marta Agnieszka (Nov. 2024). "Boundary Layer Turbulence". Available at: https://www.gfy.ku.dk/ nuterman/teamocean/index.html. PhD thesis. Tagensvej 16, Denmark: University of Copenhagen.

Poulsen, Mads Bruun (Nov. 2018). "Parameterizing Southern Ocean eddy-induced circulation in coarse resolution ocean models". Available at: https://www.gfy.ku.dk/ nuterman/teamocean/index.html. PhD thesis. Tagensvej 16, Denmark: University of Copenhagen.

Stoustrup, Aster (2024). "Automated Parameter Tuning for the Versatile Ocean Simulator (VEROS)". MA thesis. University of Copenhagen.

Vallis, Geoffrey K. (2017a). "Barotropic and Baroclinic Instability". In: Atmospheric and Oceanic Fluid Dynamics: Fundamentals and Large-Scale Circulation. Cambridge University Press, pp. 335–378.

— (2017b). "Basics of Incompressible Turbulence". In: Atmospheric and Oceanic Fluid Dynamics: Fundamentals and Large-Scale Circulation. Cambridge University Press, pp. 413–444.

— (2017c). "Geostrophic Turbulence and Baroclinic Eddies". In: Atmospheric and Oceanic Fluid Dynamics: Fundamentals and Large-Scale Circulation. Cambridge University Press, pp. 445–472.

— (2017d). "Turbulent Diffusion and Eddy Transport". In: Atmospheric and Oceanic Fluid Dynamics: Fundamentals and Large-Scale Circulation. Cambridge University Press, pp. 473–508.

9 Appendix

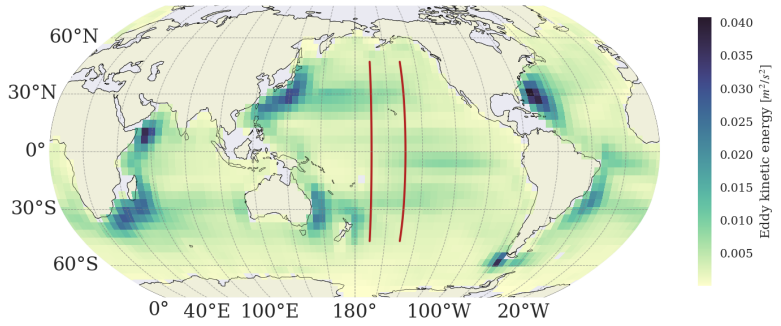

Figure 10: Area of scale analysis

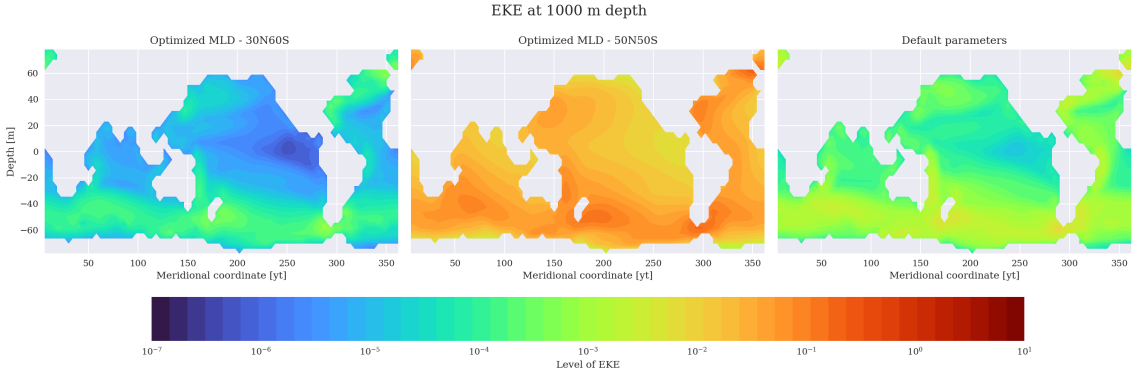

Figure 11: EKE in Latitude/longitude coordinates

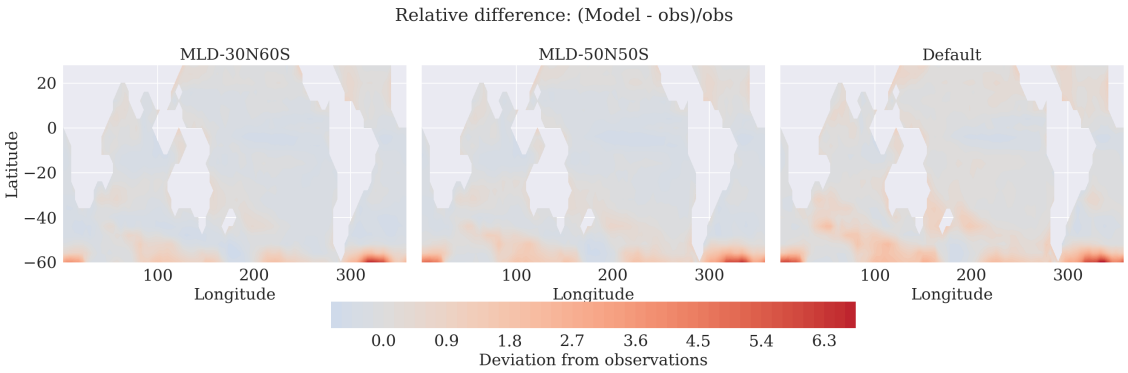

Figure 12: Mixed layer depth difference

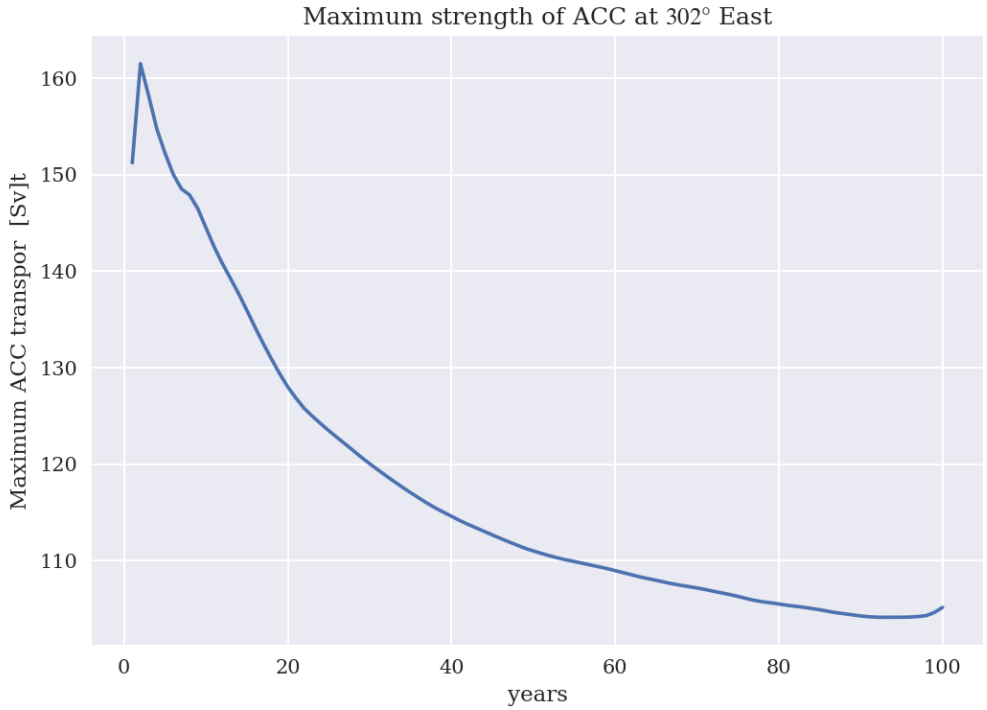

Figure 13: Spinup of the ACC

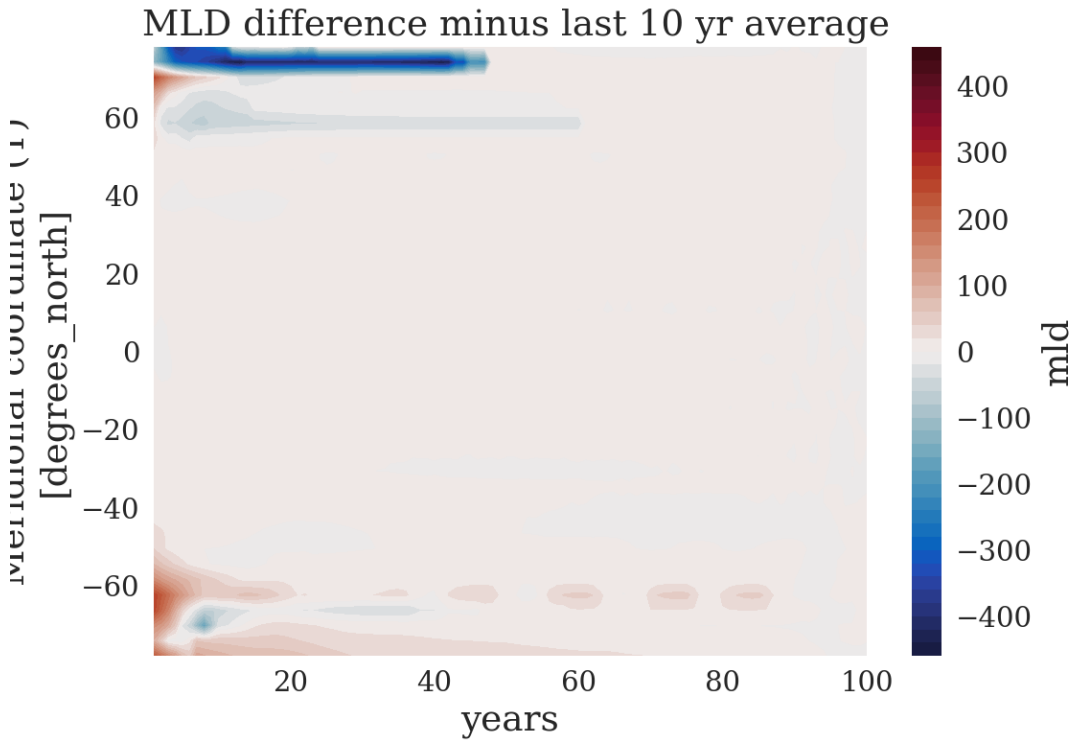

Figure 14: Spinup of the mld. Plot shows the model output of MLD with the average of the last 10 years subtracted.

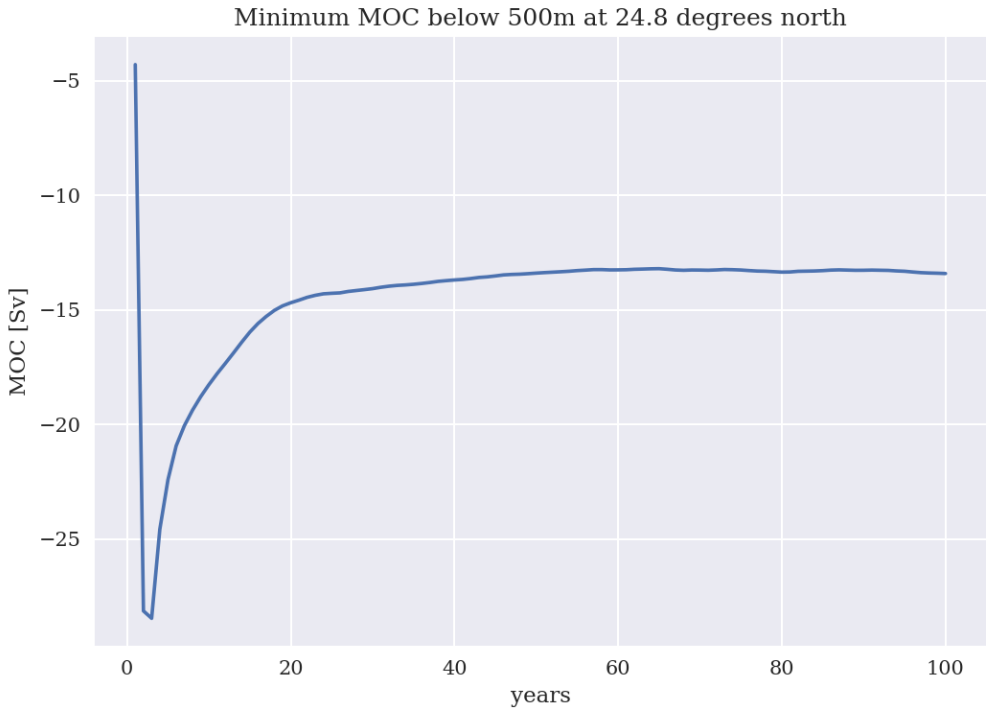

Figure 15: Mixed layer depth difference

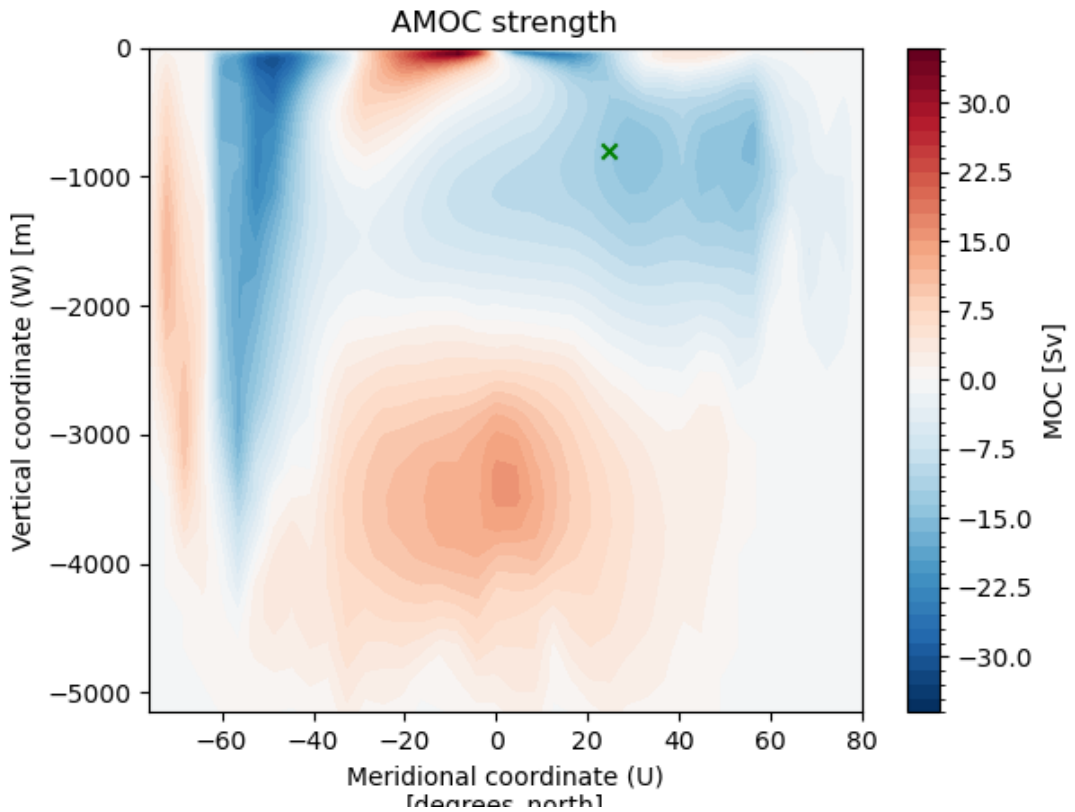

Figure 16: Figure showing where the amoc strength is monitored. For each simulation the minimum is found in the depth coordinate, at 24°north

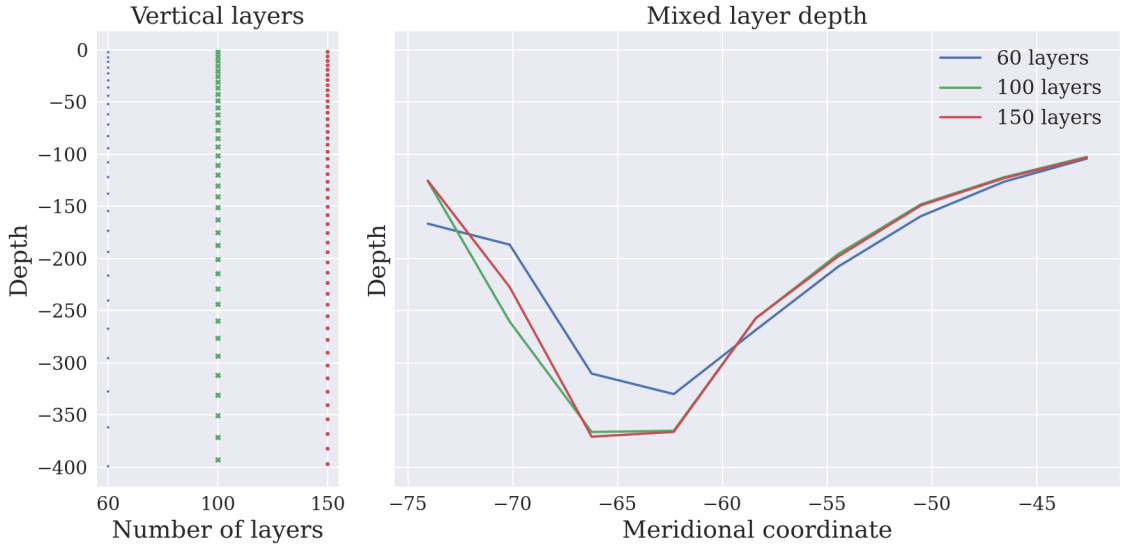

Figure 17: Vertical sensitivity to mixed layer depth for different model resolutions

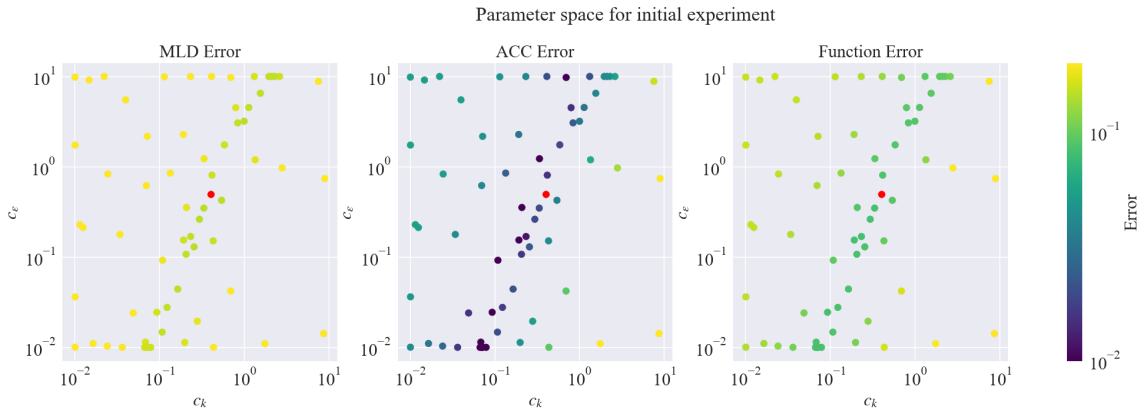

Figure 18: Parameterspace for the twin experiment